J|A|C|S
ARTICLES
Published on Web 01/05/2005

Temperature Dependence of Three-Body Hydrophobic Interactions: Potential of Mean Force, Enthalpy, Entropy, Heat Capacity, and Nonadditivity

Maria Sabaye Moghaddam, Seishi Shimizu,† and Hue Sun Chan*

Contribution from the Protein Engineering Network of Centres of Excellence (PENCE), Department of Biochemistry, and Department of Medical Genetics & Microbiology, Faculty of Medicine, University of Toronto, Toronto, Ontario M5S 1A8, Canada

Received July 1, 2004; E-mail: chan@arrhenius.med.toronto.edu

Abstract: Temperature-dependent three-body hydrophobic interactions are investigated by extensive constant-pressure simulations of methane-like nonpolar solutes in TIP4P model water at six temperatures. A multiple-body hydrophobic interaction is considered to be (i) additive, (ii) cooperative, or (iii) anti-cooperative if its potential of mean force (PMF) is (i) equal to, (ii) smaller than, or (iii) larger than the corresponding pairwise sum of two-methane PMFs. We found that three-methane hydrophobic interactions at the desolvation barrier are anti-cooperative at low to intermediate T, and vary from essentially additive to slightly cooperative at high T. Interactions at the contact minimum are slightly anti-cooperative over a wider temperature range. Enthalpy, entropy, and heat capacity are estimated from the computed PMFs. Contrary to the common expectation that burial of solvent-accessible nonpolar surface area always leads to a decrease in heat capacity, the present results show that the change in heat capacity upon three-methane association is significantly positive at the desolvation barrier and slightly positive at the contact minimum. This suggests that the heat capacity signature of a hydrophobic polymer need not vary uniformly nor monotonically with conformational compactness. Ramifications for protein folding are discussed.

I. Introduction

Hydrophobic effects underlie a wide range of physicochemical and biomolecular phenomena. In particular, hydrophobic interaction has been identified as one of the major driving forces in protein folding.[1−11] Hydrophobic interaction is an effective interaction. It refers to the solvent-mediated influence exerted on one another by nonpolar groups in water and consists of the direct interactions between the nonpolar groups as well as averaged effects of the surrounding water molecules. Traditionally, hydrophobic interactions are often described by empirical energetic parameters deduced from solvation and transfer data of model compounds[2,6,12−14] in conjunction with simple geometrical measures of aqueous exposure, such as solvent-accessible and molecular surface area.[15,16] Such "implicit-solvent" approaches[17,18] and related simple lattice constructs[11,19−21] have led to useful insights. However, as it has long been recognized, many microscopic intricacies of hydrophobic interaction, e.g., the potential of mean force (PMF) between two small nonpolar solutes,[22] cannot be captured by implicit-solvent, bulk-phase considerations,[23] nor are they readily accessible by current experimental techniques. Therefore, to gain deeper physical insights into the energetic and structural bases of hydrophobic behavior, simulations of atomic models of water are indispensable.[24,25]

Much of the current microscopic-level understanding of hydrophobicity is derived from molecular simulations of single-solute hydration and corresponding simulations of the water-mediated interaction between a pair of small nonpolar solutes.

† Present address: Structural Biology Laboratory, Department of Chemistry, The University of York, York, North Yorkshire YO10 5YW, U.K.

(1) Kauzmann, W. *Adv. Protein Chem.* **1959**, *14*, 1−63.
(2) Tanford, C. *The Hydrophobic Effect: Formation of Micelles and Biological Membranes*; Wiley: New York, 1980.
(3) Ben-Naim, A. *Hydrophobic Interactions*; Plenum: Oxford, 1980.
(4) Dill, K. A. *Biochemistry* **1990**, *29*, 7133−7155.
(5) Blokzijl, W.; Engberts, J. B. F. N. *Angew. Chem., Int. Ed. Engl.* **1993**, *32*, 1545−1579.
(6) Chan, H. S.; Dill, K. *A. Annu. Rev. Biophys. Biomol. Struct.* **1997**, *26*, 425−459.
(7) Scheraga, H. A. *J. Biomol. Struct. Dyn.* **1998**, *16*, 447−460.
(8) Hummer, G.; Garde, S.; Garcia, A. E.; Pratt, L. E. *Chem. Phys.* **2000**, *258*, 349−370.
(9) Southall, N. T.; Dill, K. A.; Haymet, A. D. J. *J. Phys. Chem. B* **2002**, *106*, 521−533; **2002**, *106*, 2812 (correction).
(10) Pratt, L. R. *Annu. Rev. Phys. Chem.* **2002**, *53*, 409−436.
(11) Widom, B.; Bhimalapuram, P.; Koga, K. *Phys. Chem. Chem. Phys.* **2003**, *5*, 3085−3093.
(12) Baldwin, R. L. *Proc. Natl. Acad. Sci. U.S.A.* **1986**, *83*, 8069−8072.
(13) Makhatadze, G. I.; Privalov, P. L. *Adv. Protein Chem.* **1995**, 47, 307−425.
(14) Myers, J. K.; Pace, C. N.; Scholtz, J. M. *Protein Sci.* **1995**, *4*, 2138−2148.
(15) Lee, B.; Richards, F. M. *J. Mol. Biol.* **1971**, *55*, 379−400.
(16) Richards, F. M. *Annu. Rev. Biophys. Bioeng.* **1977**, *6*, 151−176.
(17) Roux, B.; Simonson, T. *Biophys. Chem.* **1999**, *78*, 1−20 and references therein.
(18) Feig, M.; Brooks, C. L., III. *Curr. Opin. Struct. Biol.* **2004**, *14*, 217−224 and references therein.
(19) De Los Rios, P.; Caldarelli, G. *Phys. Rev. E* **2000**, *62*, 8449−8452.
(20) Bedeaux, D.; Koper, J. M.; Ispolatov, I.; Widom, B. *Physica A* **2001**, *291*, 39−48.
(21) Salvi, G.; De Los Rios, P. *Phys. Rev. Lett.* **2003**, *91*, 258102.
(22) Pratt, L. R.; Chandler, D. *J. Chem. Phys.* **1977**, *67*, 3683−3704.
(23) Wood, R. H.; Thompson, P. T. *Proc. Natl. Acad. Sci. U.S.A.* **1990**, *87*, 946−949.
(24) Geiger, A.; Rahman, A.; Stillinger, F. H. *J. Chem. Phys.* **1979**, *70*, 263−276.
(25) Pangali, C.; Rao, M.; Berne, B. J. *J. Chem. Phys.* **1979**, *71*, 2982−2990.

(A brief review can be found in the Introduction of ref 26.) Pairwise (two-body) PMFs have provided essential thermodynamic information for evaluating implicit-solvent potential functions, especially with regard to their ability to incorporate the physics of desolvation free energy barriers.[27−32] Recently, two-body PMFs have also led to physically plausible rationalizations of experimental conformational properties of heat- and urea-denatured states of proteins.[33,34] It has become apparent, however, that the role of hydrophobicity in protein folding is more complex than a simple summation of pairwise hydrophobic interactions.[35,36] Indeed, it has long been known that hydrophobic effects can be associated with significantly different hydrogen-bonding patterns of water molecules, depending on the length scale and surface curvature of the nonpolar solutes in question.[37−42] The core of a protein's native structure contains many nonpolar groups in a wide variety of configurations. Thus, a more complete physical picture of the protein folding process entails considerations beyond two-solute studies. While the hydrophobic component of the driving force for folding may be addressed by direct explicit-water simulations of hydrophobic collapse of model polymer chains,[43,44] to gain fundamental understanding into possible nonadditive effects at play, increasing attention is being directed toward the simulation and systematic analysis of clustering and association of three or more nonpolar solutes in water.[27,36,45−56]

In general, the main question about the additivity of hydrophobic interactions is whether the solvent-mediated interaction free energy (PMF) $W^{(m)}(\mathbf{r}_1,\mathbf{r}_2,\mathbf{r}_3,...,\mathbf{r}_m)$ among three or more nonpolar solutes in a given configuration ($\mathbf{r}$'s denote the positions of the solutes, $m \geq 3$) can be well approximated by the sum of independent two-solute PMFs. If $W^{(m)}(\mathbf{r}_1,\mathbf{r}_2,\mathbf{r}_3,...,\mathbf{r}_m) = \sum_{i<j}^{m} W^{(2)}(\mathbf{r}_i,\mathbf{r}_j)$, the interaction is pairwise additive (often referred to simply as "additive"). Otherwise, the interaction is termed cooperative or anti-cooperative, depending on whether the actual multiple-body PMF is more or less favorable to solute association than the pairwise PMF sum.[36]

Our interest in many-body hydrophobic effects[27,49] has been motivated by our effort to ascertain the physical basis of the high degree of two-state-like thermodynamic and kinetic cooperativity exhibited by many small, single-domain proteins. Although not all proteins share such properties,[57] the existence of proteins that do presents a challenge to our basic understanding of protein energetics. Apparently, at least in coarse-grained heteropolymer chain models, we find that pairwise additive interactions alone are insufficient to produce cooperative behavior resembling that of many single-domain proteins.[36,58] Many-body interactions have been used in protein modeling,[35,59−64] some of which have demonstrated an ability to enhance the thermodynamic and kinetic cooperativity of model proteins.[36] However, the relationship between the nonadditivity of the interactions among a protein's constituent groups and the protein's overall cooperative behavior can be subtle. For instance, in view of the fact that hydrophobic interaction is only one of many energetic factors in protein folding, a presumed *anti-cooperativity* of hydrophobic interactions at room temperature that disfavors the formation of conformational intermediates may, under certain circumstances, contribute to the overall thermodynamic cooperativity of the protein.[36]

Two of us have previously investigated the water-mediated interaction among three methanes at room temperature (25 °C, 298.15 K) under atmospheric pressure (1 atm). To ensure consistent zero-PMF baselines for a proper comparison between pairwise two-methane and three-methane interactions, PMFs were obtained[26] using the Widom test-particle insertion techniques.[65,66] For the class of three-methane configurations we had investigated previously, we found that three-methane interaction has non-negligible anti-cooperativity at 25 °C and 1 atm. In other words, while three-methane association in water is favored, it is favored less than that predicted by assuming the water-mediated methane interaction is pairwise additive.[27,49] Moreover, these results indicate that the nonadditive effects seen in direct molecular simulations are not adequately captured by several common schemes of implicit-solvent modeling.[27]

Here we extend our 1-atm three-methane study at 25 °C to examine six temperatures between 0 and 100 °C. The temperature dependence of free energies of hydration has been central to the characterization and rationalization of hydrophobic effects. Thermodynamic signatures such as heat capacity are crucial not only for understanding basic hydrophobic effects; they are often invoked to infer conformational changes in the study of protein

(26) Shimizu, S.; Chan, H. S. *J. Chem. Phys.* **2000**, *113*, 4683−4700; **2002**, *116*, 8636 (erratum).
(27) Shimizu, S.; Chan, H. S. *Proteins* **2002**, *48*, 15−30; **2002**, *49*, 294 (erratum).
(28) Cheung, M. S.; Garcia, A. E.; Onuchic, J. N. *Proc. Natl. Acad. Sci. U.S.A.* **2002**, *99*, 685−690.
(29) Kaya, H.; Chan, H. S. *J. Mol. Biol.* **2003**, *326*, 911−931; **2004**, *337*, 1069 (corrigendum).
(30) Masunov, A.; Lazaridis, T. *J. Am. Chem. Soc.* **2003**, *125*, 1722−1730.
(31) Zhou, R. H. *Proteins* **2003**, *53*, 148−161.
(32) Guo, W.; Lampoudi, S.; Shea, J.-E. *Proteins* **2004**, *55*, 395−406.
(33) Shimizu S.; Chan, H. S. *J. Am. Chem. Soc.* **2001**, *123*, 2083−2084.
(34) Shimizu, S.; Chan, H. S. *Proteins* **2002**, *49*, 560−566.
(35) Chan, H. S. *Proteins* **2000**, *40*, 543−571.
(36) Chan, H. S.; Shimizu, S.; Kaya, H. *Methods Enzymol.* **2004**, *380*, 350−379.
(37) Lee, C. Y.; McCammon, J. A.; Rossky, P. J. *J. Chem. Phys.* **1984**, *80*, 4448−4455.
(38) Lum, K.; Chandler, D.; Weeks, J. D. *J. Phys. Chem. B* **1999**, *103*, 4570−4577.
(39) Southall, N. T.; Dill, K. A. *J. Phys. Chem. B* **2000**, *104*, 1326−1331.
(40) Southall, N. T.; Dill, K. A. *Biophys. Chem.* **2002**, *101*, 295−307.
(41) Leung, K.; Luzar, A.; Bratko, D. *Phys. Rev. Lett.* **2003**, *90*, 065502.
(42) Huang, X.; Margulis, C. J.; Berne, B. J. *J. Phys. Chem. B* **2003**, *107*, 11742−11748.
(43) Mountain, R. D.; Thirumalai, D. *J. Am. Chem. Soc.* **2003**, *125*, 1950−1957.
(44) Collet, O.; Chipot, C. *J. Am. Chem. Soc.* **2003**, *125*, 6573−6580.
(45) Rank, J. A.; Baker, D. *Protein Sci.* **1997**, *6*, 347−354.
(46) Tsai, J.; Gerstein, M.; Levitt, M. *Protein Sci.* **1997**, *6*, 2606−2616.
(47) Martorana, V.; Bulone, D.; San Biagio, P. L.; Palma-Vittorelli, M. B.; Palma, M. U. *Biophys. J.* **1997**, *73*, 31−37.
(48) Czaplewski, C.; Rodziewicz-Motowidlo, S.; Liwo, A.; Ripoll, D. R.; Wawak, R. J.;Scheraga, H. A. *Protein Sci.* **2000**, *9*, 1235−1245.
(49) Shimizu, S.; Chan, H. S. *J. Chem. Phys.* **2001**, *115*, 1414−1421.
(50) Raschke, T. M.; Tsai, J.; Levitt, M. *Proc. Natl. Acad. Sci. U.S.A.* **2001**, *98*, 5965−5969.
(51) Czaplewski, C.; Rodziewicz-Motowidlo, S.; Liwo, A.; Ripoll, D. R.; Wawak, R. J.; Scheraga, H. *A. J. Chem. Phys.* **2002**, *116*, 2665−2667.
(52) Shimizu, S.; Chan, H. S. *J. Chem. Phys.* **2002**, *116*, 2668−2669.
(53) Czaplewski, C.; Ripoll, D. R.; Liwo, A.; Rodziewicz-Motowidlo, S.; Wawak, R. J.; Scheraga, H. A. *Int. J. Quantum Chem.* **2002**, *88*, 41−45.
(54) Yang, H. B.; Elcock, A. H. *J. Am. Chem. Soc.* **2003**, *125*, 13968−13969.
(55) Ghosh, T.; Garcia, A. E.; Garde, S. *J. Phys. Chem. B* **2003**, *107*, 612−617.
(56) Czaplewski, C.; Rodziewicz-Motowidlo, S.; Dabal, M.; Ripoll, D. R.; Scheraga, H. A. *Biophys. Chem.* **2003**, *105*, 339−359.
(57) Garcia-Mira, M. M.; Sadqi, M.; Fischer, N.; Sanchez-Ruiz, J. M.; Muñoz, V. *Science* **2002**, *298*, 2191−2195.
(58) Scalley-Kim, M.; Baker, D. *J. Mol. Biol.* **2004**, *338*, 573−583.
(59) Plotkin, S. S.; Wang, J.; Wolynes, P. *G. J. Chem. Phys.* **1997**, *106*, 2932−2948.
(60) Takada, S.; Luthey-Schulten, Z.; Wolynes, P. G. *J. Chem. Phys.* **1999**, *110*, 11616−11629.
(61) Kaya, H.; Chan, H. S. *Proteins* **2000**, *40*, 637−661; **2001**, *43*, 523 (erratum).
(62) Kaya, H.; Chan, H. S. *Phys. Rev. Lett.* **2000**, *85*, 4823−4826.
(63) Eastwood, M. P.; Wolynes, P. *G. J. Chem. Phys.* **2001**, *114*, 4702−4716.
(64) Pokarowski, P.; Kolinski, A.; Skolnick, J. *Biophys. J.* **2003**, *84*, 1518−1526.
(65) Widom, B. *J. Chem. Phys.* **1963**, *39*, 2808−2812.
(66) Forsman, J.; Jönsson, B. *J. Chem. Phys.* **1994**, *101*, 5116−5125.

folding.[4,12−14,67−73] Several groups have conducted molecular simulations of temperature-dependent hydrophobic interactions in recent years.[26,33,34,36,40,74−78] (Earlier efforts are briefly reviewed in ref 26.) These investigations have revealed previously unknown intricacies. Most noteworthy is that the heat capacity change associated with bringing a pair of small nonpolar solutes from infinite separation to the position at the desolvation free energy barrier is significantly positive. This feature appears to be robust across several common water models[77] and is applicable to a number of different small hydrophobic solutes, including methanes,[26,33,34,76] xenons,[77,78] and small nonpolar solutes in a two-dimensional model of water.[40] The phenomenon is contrary to the prediction from conventional solvent-accessible surface area that the heat capacity change associated with hydrophobic association and burial of any nonpolar surface should always be negative. It underscores that the difference between pair and bulk hydrophobic effects[23] can be striking.[33,34]

The present calculation of temperature-dependent, three-body PMFs enables us to estimate the entropy, enthalpy, and heat capacity changes associated with three-methane interactions in water. To our knowledge, these thermodynamic signatures of three-body hydrophobic interactions have not been determined before. Similar to the two-methane case, prominent positive heat capacity values are observed at the three-methane desolvation barrier region. Moreover, we find that the sign of nonadditivity of three-methane interactions is sensitive to temperature. In the present TIP4P model, the contact minimum appears to be consistently anti-cooperative, except perhaps at very low temperatures, but the desolvation barrier shifts from mainly anti-cooperative at low and intermediate temperatures toward more pairwise additive and slightly cooperative behavior at high temperatures. Details of these findings and their implications are discussed below.

II. Computational Methods

We begin by summarizing the computational approach used in the present investigation. Following previous studies from our group, results in this work are obtained by constant-pressure, constant-temperature (*NPT*) Monte Carlo simulations of 396 TIP4P water molecules under 1 atm at six different temperatures ranging from 5 to 95 °C using BOSS version 4.1.[79] The temperatures studied are 278.15 K (5 °C), 298.15 K (25 °C), 313.15 K (40 °C), 328.15 K (55 °C), 348.15 K (75 °C), and 368.15 K (95 °C). For brevity in subsequent discussions, these temperatures will be referred to respectively as 278, 298, 313, 328, 348, and 368 K. Details of the simulation methodology have been given in ref 26. Only a summary of the salient features will be provided below. The model system (Figure 1) and all numerical parameters used in this article are the same as those in the work of Shimizu and Chan.[27] In particular, a united-atom representation is used for the methanes. The parameters (σ, ϵ) in the Lennard-Jones potential $4\epsilon[(\sigma/r)^{12} - (\sigma/r)^6]$, in units of (Å, kcal/mol), for water−water, methane−methane, and water−methane interactions, are (3.15365, 0.1550), (3.730, 0.294), and (3.44183, 0.2135), respectively. The simulation box size is approximately 23 Å × 23 Å × 23 Å and is subjected to variation in accordance with the constant-pressure constraint, and periodic boundary conditions are applied. The cutoff distance of water−water and water−methane interactions is 9.0 Å in our simulations.[26] Ewald summation is not used because the TIP4P water model[80] was thermodynamically parametrized by using cutoffs for electrostatic interactions without Ewald summations, as has been underscored in recent studies of three-methane PMFs.[27,48] We note that cutoffs of electrostatic interactions without Ewald summations have been employed in several other PMF studies as well (see ref 27 and references therein).

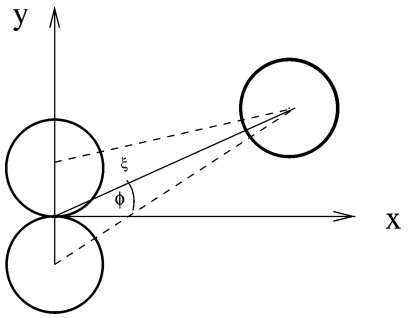

Figure 1. Three-methane system studied in this work. Methanes are shown as spheres of radius 1.9 Å; water molecules are not shown. The geometrical variables ϕ and ξ define the relative position of the single methane and the methane dimer; x and y are Cartesian coordinates.

Figure 1 provides the geometrical variables used in the present work. Simulations are performed for seven values of ϕ (= 0, π/12, π/6, π/4, π/3, 5π/12, π/2). We use the same test-particle insertion method[65,66] as in our previous studies.[26,27,49] At each temperature, three-methane PMFs are obtained as the difference of two quantities:

$$\mathrm{PMF} = \Delta G(\xi,\phi) = \mu^*_{abc}(\xi,\phi) - \mu^*_a \tag{1}$$

where $\mu^*_{abc}(\xi,\phi)$ is the free energy of inserting a single methane (labeled *a*) into an aqueous environment at a specific position (defined by ξ,ϕ) relative to the fixed methane dimer (labeled *b*,*c*), and μ^*_a is the (hydration) free energy of inserting a single methane into a given position in pure water. The single-methane hydration free energy is given by

$$\mu^*_a = -kT \ln\left[\frac{\langle V \exp(-U_a/kT)\rangle_N}{\langle V\rangle_N}\right] \tag{2}$$

where kT is Boltzmann constant times absolute temperature, U_a is the interaction energy between the single methane and all of the water molecules, V is the (variable) volume of the simulation box for the given configuration, and $\langle ...\rangle_N$ denotes averaging over the degrees of freedom of N = 396 water molecules under the constant-pressure (P) constraint. This averaging is computed by using a weighting factor equal to $\exp(-PV/kT)$ times the Boltzmann factor for the water−water potential energy.[26] Following the formulation on page 1416 in the work by Shimizu and Chan,[49] the three-methane insertion free energy is obtained by the relation

$$\mu^*_{abc}(\xi,\phi) = -kT \ln\left[\frac{\langle V \exp\{-[U_a + U_{abc}(\xi,\phi)]/kT\}\rangle_{N,bc}}{\langle V\rangle_{N,bc}}\right] \tag{3}$$

where $\langle ...\rangle_{N,bc}$ here stands for averaging over the configurations of N

(67) Sturtevant, J. M. *Proc. Natl. Acad. Sci. U.S.A.* **1977**, *74*, 2236−2240.
(68) Privalov, P. L.; Gill, S. J. *Adv. Protein Chem.* **1988**, *39*, 191−234.
(69) Makhatadze, G. I.; Privalov, P. *L. J. Mol. Biol.* **1990**, *213*, 375−384.
(70) Murphy, K. P.; Freire, E. *Adv. Protein Chem.* **1992**, *43*, 313−361.
(71) Spolar, R. S.; Livingstone, J. R.; Record, M. T. *Biochemistry* **1992**, *31*, 3947−3955.
(72) Gomez, J.; Hilser, V. J.; Xie, D.; Freire, E. *Proteins* **1995**, *22*, 404−412.
(73) Loladze, V. V.; Ermolenko, D. N.; Makhatadze, G. I. *Protein. Sci.* **2001**, *10*, 1343−1352.
(74) Rick, S. W. *J. Phys. Chem. B* **2000**, *104*, 6884−6888.
(75) Ghosh, T.; Garcia, A. E.; Garde, S. *J. Chem. Phys.* **2002**, *116*, 2480−2486.
(76) Rick, S. W. *J. Phys. Chem. B* **2003**, *107*, 9853−9857.
(77) Paschek, D. *J. Chem. Phys.* **2004**, *120*, 6674−6690.
(78) Paschek, D. *J. Chem. Phys.* **2004**, *120*, 10605−10617.
(79) Jorgensen, W. *L. BOSS*, Version 4.1; Yale University: New Haven, CT, 1999.
(80) Jorgensen, W. L.; Chandrasekhar, J.; Madura, J. D.; Impey, R. W.; Klein, M. L. *J. Chem. Phys.* **1983**, *79*, 926−935.

Table 1. Temperature Dependence of Single-Methane Hydration Free Energy μ_a^* in the TIP4P Model at 1 atm

T (K)	μ_a^* (kcal/mol)	sampling uncertainty (kcal/mol)
278	2.089	±0.002
298[a]	2.326	±0.005
313	2.4788	±0.0005
328	2.583	±0.005
348	2.71038	±0.00003
368	2.762	±0.003

[a] $T = 298$K data is from ref 27.

water molecules in the presence of a fixed methane dimer *b*,*c*, and $U_{abc}(\xi,\phi)$ is the direct interaction energy between the single methane *a* and the methane dimer *b*,*c*.

A defining feature of the test-particle insertion method is that the computation for the single-methane μ_a^* is independent of that for the three-methane $\mu_{abc}^*(\xi,\phi)$. Physically, the spatial range of hydrophobic interaction is expected to be finite, although how far apart two nonpolar groups need to be separated in water before they have negligible effects on one another is not yet accurately known.[81] It follows that placing a single methane in water at a position infinitely far away from a methane dimer should have the same free energy as placing the single methane into pure water. In other words, while by definition μ_a^* itself does not depend on the methane's position in water, $\mu_a^* = \lim_{\xi\to\infty} \mu_{abc}^*(\xi,\phi)$ is expected. Hence, by construction, the three-methane PMF given by eq 1 possesses an unambiguous zero-PMF baseline which corresponds to the nonexistent interaction between a single methane infinitely separated from a methane dimer.

To compute the quantity defined by eqs 2 and 3, we first use Monte Carlo sampling to generate a large collection of configurations of water molecules, both in the absence and in the presence of a fixed methane dimer. Monte Carlo moves attempted in these samplings of water configurations consist of translational and rotational displacements as well as volume moves, all of which are identical to those described before.[26] In the present simulations, one pass equals 396 Monte Carlo steps. In each run for the calculation of μ_{abc}^*, 1.5×10^5 initial (equilibrating) passes are discarded. Subsequently, coordinates (snapshots) of the methane dimer solution are collected every 10 passes over a course of 5.3×10^7 passes. An estimation of the statistical inefficiency of our sampling indicates that each such simulation generates roughly 10^4 uncorrelated blocks of data of water configurations.[82] Insertions of a single methane into the snapshots are then attempted at seven ϕ values ($\phi = n\pi/12$, $n = 0, 1, ..., 6$). For each ϕ, 1000 insertions are attempted per snapshot at different ξ positions to estimate the ensemble averages in eq 3.

III. Results

A. Setting the Zero-PMF Baselines: Temperature Dependence of Single-Methane Hydration. Since the single-methane hydration free energy μ_a^* is essential to the present test-particle insertion techniques as a reference free energy for PMFs at infinite separation and thus its accuracy is crucial, we have recomputed μ_a^* for $T = 278$, 313, 328, 348, and 368 K. Approximately 1.3×10^7 passes are performed here for each temperature, and sampling uncertainties are estimated by comparing half-simulation and full-simulation results (Table 1).

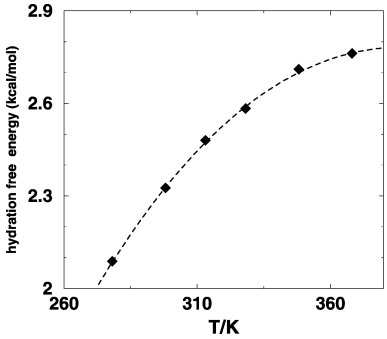

Figure 2. Single-methane hydration free energy μ_a^* as a function of temperature. Filled diamonds are simulation data points from Table 1. The dashed curve is the least-squares fit described in the text with hydration heat capacity $\Delta C_P = 41.07$ cal mol^{-1} K^{-1}. The root-mean-square deviation of the simulated free energies to the fit is 0.0055 kcal mol^{-1} K^{-1}.

The free energies thus obtained have reduced uncertainties, and they are consistent with our previous results.[26,83] The single-methane hydration free energy at 298 K has been determined to be 2.326 ± 0.006 kcal/mol in our previous work.[27] This $T =$ 298 K result is consistent with a more recent independent TIP4P simulation by Paschek[77] that yielded a corresponding free energy of 2.340 ± 0.024 kcal/mol for 300 K.

Enthalpy, entropy, and heat capacity of single-methane hydration are estimated by least-square fitting the simulation results of free energy to[26]

$$\Delta G(T) = \Delta H_0 + (T - T_0)\Delta C_P - T\Delta S_0 - T\Delta C_P \ln\left(\frac{T}{T_0}\right) \quad (4)$$

where ΔH_0 and ΔS_0 are enthalpy and entropy changes, respectively, at a given reference temperature T_0, and the constant-pressure heat capacity change ΔC_P associated with the process is taken to be temperature independent. In other words, three (output) parameters ΔH_0, ΔS_0, and ΔC_P are determined by fitting the simulated free energies, $\Delta G(T)$'s at different temperatures, as the input. Figure 2 shows that eq 4 provides a good fit to the simulated free energies, yielding $\Delta H_0 = -0.862$ kcal/mol and $\Delta S_0 = -10.7$ cal mol^{-1} K^{-1} for $T_0 = 25$ °C, and $\Delta C_P = 41.1$ cal mol^{-1} K^{-1}. The ΔS_0 and ΔC_P determined here are in close agreement with those reported by Shimizu and Chan, who found these values to be −9.72 cal mol^{-1} K^{-1} and 40.1 cal mol^{-1} K^{-1}, respectively.[26] The present ΔH_0, however, is significantly larger in magnitude than Shimizu and Chan's value of −0.562 kcal/mol. Our $\Delta S_0 = -10.7$ cal mol^{-1} K^{-1} is also consistent with a recent extensive study by Paschek that led to a corresponding value of −47 ± 5 J mol^{-1} K^{-1} (−11.2 ±1.2 cal mol^{-1} K^{-1}) for methane in TIP4P water at 300 K. Our simulated ΔG value of ∼2.3 kcal/mol for 298 K is in reasonable agreement with experiment: both Widom et al.[11] and Rettich et al.[84,85] reported ∼2.0 kcal/mol for the experimental hydration free energy for methane at $T = 298$ or 300 K. The signs of our simulated ΔS_0 and ΔH_0 agree with experimental measurements. However, the magnitude of the simulated ΔS_0 is smaller than the corresponding experimental values of ∼ −16.7 cal mol^{-1}

(81) Leikin, S.; Parsegian, V. A.; Rau, D. C.; Rand, R. P. *Annu. Rev. Phys. Chem.* **1993**, *44*, 369−395.

(82) For the two-methane PMF calculation we have conducted, wherein snapshots of water configurations were taken every 100 passes, the statistical inefficiency parameter *s* (see, e.g., Allen, M. P.; Tildesley, D. J. *Computer Simulation of Liquids*; Oxford University Press: Oxford, 1987) was determined to range from $s \approx 75$ for low and intermediate T (below 328 K) to $s \approx 35$ for high T (348, 368 K). It follows that, during the course of our simulation, water configuations become uncorrelated after roughly 4000−7000 passes of sampling.

(83) The temperature-dependent reference-state single-methane hydration free energy μ_a^* in pure water for the present model at 1 atm was previously determined,[26] in units of kcal/mol, to be 2.11 ± 0.06 (278 K), 2.34 ± 0.05 (298 K), 2.48 ± 0.08 (313 K), 2.56 ± 0.06 (328 K), 2.69 ± 0.06 (348 K), and 2.71 ± 0.06 (368 K).

(84) Rettich, T. R.; Handa, Y. P.; Battino, R.; Wilhelm E. *J. Phys. Chem.* **1981**, *85*, 3230−3237.

K^{-1} reported by Widom et al.[11] and ~ -15.0 cal mol^{-1} K^{-1} deduced from the data of Rettich et al.[84,85] The magnitude of our simulated ΔH_0 is also significantly smaller than the corresponding experimental values of approximately -13 kJ/mol (~ -3 kcal/mol).[11,84−86] Apparently, further improvement in water models would be necessary to reduce these discrepancies, as none of the common water models can reproduce the temperature dependence of single-methane ΔH and ΔS over a wide temperature range.[77]

In contrast to these relatively large differences between simulated and experimental ΔH_0 and ΔS_0 magnitudes, the present simulated $\Delta C_P = 41.1$ cal mol^{-1} K^{-1} for methane in water is in reasonable agreement with several experiments.[86,87] This suggests that the heat capacity trend observed in the present model study may be more reliable. Experimentally, methane hydration ΔC_P at 298.15 K was determined using solubility measurements reported by Rettich et al.[84,85] to be $\sim$237 J mol^{-1} K^{-1} (56.7 cal mol^{-1} K^{-1}). A very similar value equivalent to 57.7 cal mol^{-1} K^{-1} at 300 K was also reported in a recent review by Widom et al.,[11] whereas a smaller value of 209 J mol^{-1} K^{-1} (48.1 cal mol^{-1} K^{-1}) at 298.15 K was determined calorimetrically by Naghibi et al.[86]

Experiments have shown that the hydration heat capacity of methane is temperature dependent,[84,86,88] varying approximately linearly in T from $\sim$65 cal mol^{-1} K^{-1} at 273 K to $\sim$40 cal mol^{-1} K^{-1} at 373 K (i.e., an $\sim$40% variation).[84] However, the present set of simulation data is insufficient for determining a temperature-dependent $\Delta C_P(T)$. This is because the three-parameter eq 4 is already a very good fit for our data: the root-mean-square deviation from the fit (Figure 2) is comparable to the largest of the sampling uncertainties in the simulated dataset (Table 1). Hence, attempting to extract a temperature dependence of ΔC_P by fitting with a fourth parameter is not justified for this set of data. In view of this computational consideration, all heat capacities in the present study are estimated by assuming that they are temperature independent. Despite this limitation, it is gratifying to note from the above comparison that our ΔC_P of single-methane hydration, estimated from multiple-temperature simulation, does lie within the experimental variations in the same temperature range.

B. Three-Methane PMFs: Degree of Deviation from Pairwise Additivity Is Temperature Dependent. Using the single-methane hydration free energy in Figure 2 to set zero-PMF baselines, we apply test-particle insertion techniques (eq 3) to the three-methane system in Figure 1 to investigate the temperature dependence of three-methane hydrophobic interactions (Figure 3).[89] Simulation data are obtained here for several values of the ϕ angle. We illustrate most of the three-methane results in this article (Figure 3 included) by the $\phi = 0$ case because certain three-methane results for this geometry from other studies are available for comparison (see below).[45,48,55,56] Computationally, the $\phi = 0$ geometry also affords a larger area for test-particle insertion, and thus the resulting simulation data are less prone to statistical uncertainty. (At $\phi = \pi/2$, for example, sampling is limited to a line as opposed to a two-dimensional conic surface for $\phi < \pi/2$.)

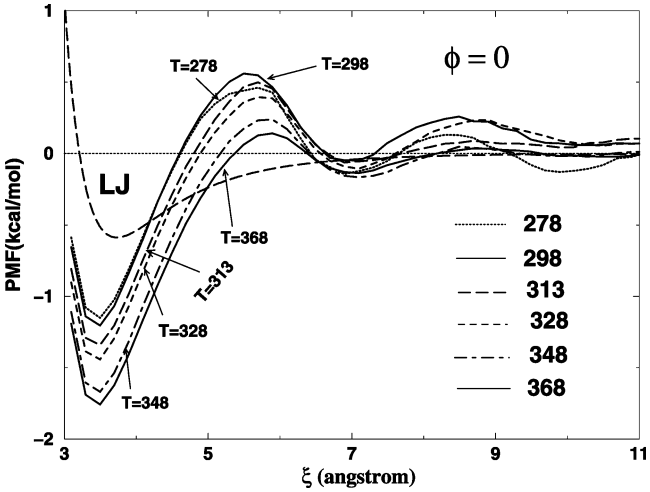

Figure 3. Three-methane PMF as a function of the intersolute separation ξ for $\phi = 0$ at six different temperatures (in kelvin) and 1 atm. The contribution from direct Lennard-Jones interactions among the methanes is also plotted for comparison (curve labeled LJ). In this and subsequent PMF figures, free energies computed by test-particle insertions are binned into 50 intervals of ξ, and an average is taken for the 20 free energies within each bin. PMF curves are then constructed by connecting the average free energies for successive bins.

Figure 3 shows the temperature dependence of three-methane PMFs. At every temperature, three distinct features are observed: a contact minimum (cm), a desolvation barrier (db), and a solvent-separated minimum (ssm). The exact locations of these features are slightly different at different temperatures. The three-methane PMFs here share two salient trends with two-methane PMFs:[26] (i) The contact minimum at $\xi \approx 3.5$ Å deepens with increasing temperature. In other words, three-methane contact interaction becomes increasingly favorable at higher temperatures. (ii) The height of the desolvation barrier at $\xi \approx 5.5$ Å decreases at high temperatures.

Whereas the results in Figure 3 pertain only to a specific set of spatial configurations of a three-methane cluster defined by $\phi = 0$, the general trend observed persists for different configurations of the methane dimer + single methane system (other values of ϕ). The geometry of the present three-methane system leads naturally to shifts of key features of the free energy profile (cm, db, and ssm) to larger values of ξ as ϕ increases from zero to $\pi/2$. At the same time, since the three-methane system cannot form an optimally packed cluster for angles other than $\phi = 0$, the stability of the contact minimum tends to decrease (free energy less negative) as ϕ increases (not all simulation data are shown). Detailed data for the angle (ϕ)

(85) Here, values of the thermodynamic quantities ΔG, ΔH_0, ΔS_0, and ΔC_P for single-methane hydration are obtained from the experiments of Rettich et al. (ref 84) by using the data in their Table 7 in conjunction with their eq 30, noting that $\Delta\mu^\circ$ in this equation is equivalent to our ΔG. Alternatively, assuming that PV-type effects are negligible in the liquid phase, the same quantities can be deduced from Table 5 of Rettich et al. by noting that, because of the difference in standard state, our ΔG is related to their ΔG_2° by $\Delta G \approx \Delta G_2^\circ + kT \ln(P_{atm}/kT\rho_w)$, where P_{atm} is atmospheric pressure and ρ_w is the (number) density of water. Analogous relationships between our ΔH, ΔS, ΔC_P and their ΔH_2°, ΔS_2°, ΔC_{P2}° are readily derived by using standard thermodynamic relations $\Delta H = -T^2\partial\Delta(G/T)/\partial T$, etc. We have verified that thermodynamic quantities calculated using these two alternate methods from the data of Rettich et al. are consistent with each other.

(86) Naghibi, H.; Dec, S. F.; Gill, S. *J. J. Phys. Chem.* **1986**, *90*, 4621−4623.

(87) Morrison, T. J.; Billett, F. *J. Chem. Soc.* **1952**, 3819−3822.

(88) Glew, D. *N. J. Phys. Chem.* **1962**, *66*, 605−609.

(89) It is clear from Figure 1 that different ϕ angles define physically different sets of relative positions for the three methanes. It should also be noted that, as in our previous studies, the PMF at a given ξ,ϕ is defined here by the free energy of insertion at a particular spatial position. By construction, this PMF does not involve entropic free energy associated with the multiplicity of methane spatial positions sharing a given ξ,ϕ. In other words, the present PMF contains no "cratic" contribution arising from the configurational degrees of freedom of the methane molecules.

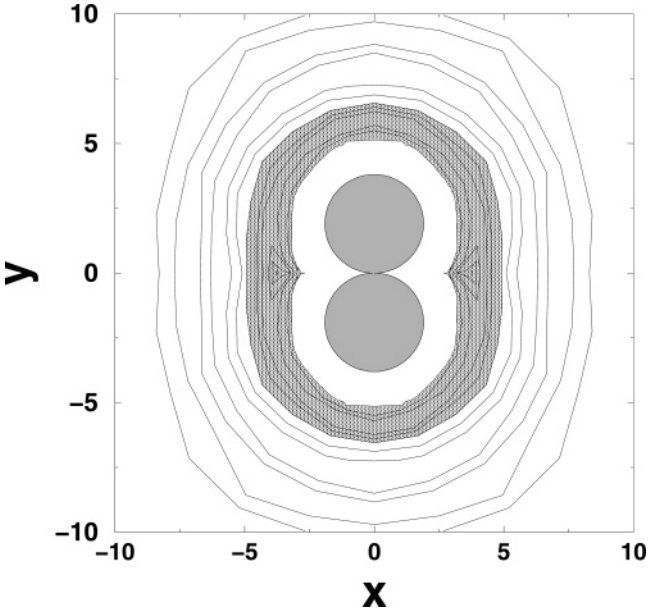

Figure 4. Contour representation of three-methane free energy landscape at 368 K (95 °C) and 1 atm on a plane defined by the *x*,*y* Cartesian coordinates in Figure 1. This plot is constructed using all three-methane simulation data for 368 K collected in this work (positive ϕ's plus the $\phi = 0$, $T = 368$ K data shown in Figure 3) and simple interpolations between simulation datapoints. The methane dimer is depicted here by the two shaded cicles; Cartesian distances are given in units of Å. Contours are shown at 0.25 kcal/mol intervals (at 0.0, −0.25, ...). They indicate the free energy of bringing a single methane to a given position in the proximity of the methane dimer from an initial distance infinitely far away. Areas with free energy ≤−0.25 kcal/mol are shaded. The corresponding contour plot for a lower temperature (25 °C) was previously provided as Figure 2A in the work of Shimizu and Chan.[27]

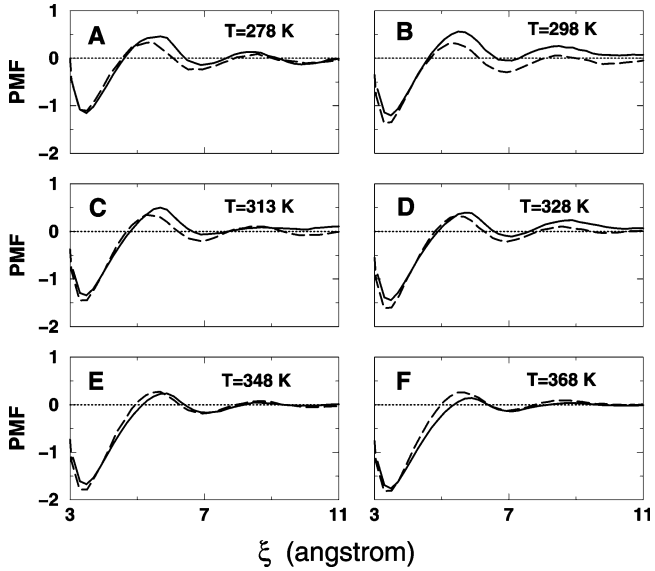

Figure 5. Three-methane PMFs (solid curves) for $\phi = 0$ at six different temperatures, compared with the corresponding hypothetical PMFs that assume pairwise additivity (dashed curves). The thin dotted lines mark the zero-PMF baseline. The $T = 298$ K results are from ref 27. Additivity-assumed PMFs at each of the other temperatures are computed using our previous two-methane method[26] from approximately 3.6×10^8 simulation passes.

dependence of three-methane PMF have been presented elsewhere for 25 °C.[27]

A more global view of the three-methane free energy landscape at a higher temperature is provided here in Figure 4 for 95 °C. The free energy contact minimum region (trench) is deeper at 95 °C than at 25 °C. However, a detailed comparison with the corresponding contour plot[27] for 25 °C indicates that, in a broad area farther away from the methane dimer, the 95 °C landscape is flatter and less rugged, and appears to have less prominent topographical features than the corresponding 25 °C landscape.

Figure 5 compares the three-methane PMFs for $\phi = 0$ at six different temperatures (solid curves) with the corresponding hypothetical PMFs that assume pairwise additivity (dashed curves). In general, for any given ξ, ϕ, and T, the hypothetical additivity-assumed three-methane PMF for the present system is defined[27] as $\Delta G_{\text{add}}(\xi,\phi) \equiv \Delta G_2(\xi_1,T) + \Delta G_2(\xi_2,T)$, where $\Delta G_2(\zeta,T)$ is the PMF at temperature T of a pair of methanes with center-of-mass separation ζ. The variables ξ_1 and ξ_2 are respectively the separations between the single methane with one methane and the other methane that constitute the methane dimer; these separations are readily determined by ξ and ϕ in Figure 1. The additivity-assumed PMFs in Figure 5 are constructed as before[26,33] using the single-methane baseline in Table 1 and additional test-particle sampling for two-methane PMFs.

Following the general definition above, three-methane hydrophobic interaction in a given ξ,ϕ configuration is considered to be (i) additive, (ii) cooperative, or (iii) anti-cooperative if the simulated three-methane PMF $\Delta G(\xi,\phi)$ in eq 1 is (i) equal to, (ii) smaller (i.e., less positive or more negative) than, or (iii) larger (i.e., more positive or less negative) than the additivity-assumed $\Delta G_{\text{add}}(\xi,\phi)$.[27,36,49] To our knowledge, the present study is the first explicit-water investigation of the temperature dependence of pairwise additivity of hydrophobic interactions. Our results in Figure 5 suggest that hydrophobic nonadditivity is significantly temperature dependent.

Because the nonadditivity effects of three-methane hydrophobic interactions are not large (see Figure 5), it is essential that sufficient Monte Carlo simulation is performed to minimize sampling uncertainty. As in part of our previous studies,[27,49] sampling uncertainties are estimated here by comparing half-simulation and full-simulation results (cf. Table 1). For the six temperatures simulated, the ranges of the magnitudes of the uncertainties of $\mu^*_{abc}(\xi,\phi = 0)$ are 0.0014−0.0236 kcal/mol at the contact minimum ($\xi \approx 3.5$ Å) and 0.005−0.0733 kcal/mol at the desolvation barrier ($\xi \approx 5.5$ Å). As detailed elsewhere,[27,51,52] the sampling uncertainty of any given nonadditivity measure, defined as the difference between a three-methane PMF and an additivity-assumed PMF, is equal to a sum of three contributions, namely (i) the sampling uncertainty of the three-methane μ^*_{abc}, (ii) two times the uncertainty of the individual two-methane μ^*_{ab} in the additivity-assumed PMF, and (iii) the sampling uncertainty of single-methane hydration free energy μ^*_a. Representative values of these uncertainties in nonadditivity estimates are reported below after "±" signs.

Our simulation data indicate that three-methane hydrophobic interaction is mainly anti-cooperative at the contact minimum (cm). Although the degree of cm anti-cooperativity is temperature dependent, it does not vary sharply with temperature. As can be seen from Figure 5, the three-methane cm free energy minus the additivity-assumed cm free energy is positive for five of the six temperatures studied. This measure of anti-cooperativity amounts to ∼0.11−0.17 kcal/mol at intermediate tem-

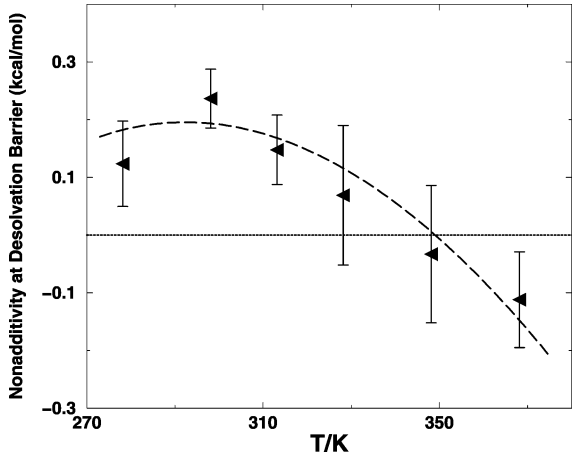

Figure 6. Temperature-dependent nonadditivity effects at the $\phi = 0$ three-methane desolvation barrier. At each of the six temperatures studied, the solid triangle represents the difference between the peak value of the simulated three-methane desolvation free energy barrier and the peak value of the desolvation barrier of the hypothetical additivity-assumed three-methane PMF (the former minus the latter; these two peaks can be at slightly different positions, cf. Figure 5.) Sampling uncertainties are estimated as described in the text and indicated by the error bars. The horizontal dotted line marks the level at which the actually simulated three-methane desolvation barrier has the same height as its hypothetical additivity-assumed counterpart. The dashed curve is merely a guide for the eye.

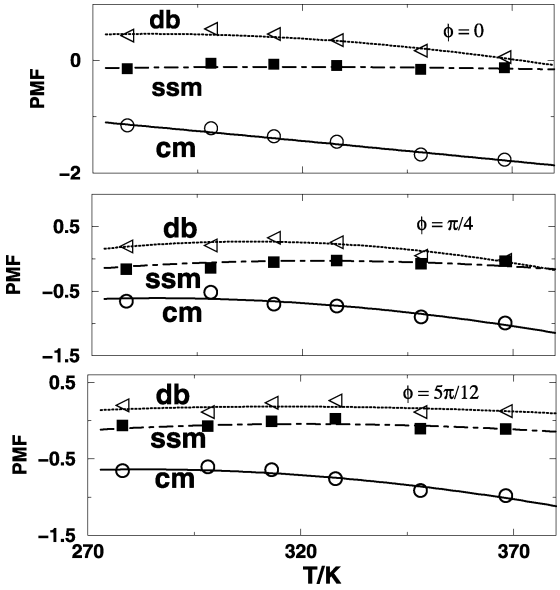

Figure 7. Temperature dependence of PMF at three classes of key positions: contact minimum (cm, circles), desolvation barrier (db, triangles), and solvent-separated minimum (ssm, squares). Examples are shown for three ϕ values as indicated. The precise ξ values of these positions for different ϕ's are provided in Figure 10. The symbols here denote simulated PMF values (free energies). The continuous curves are least-squares fits of the free energies using eq 4.

peratures (0.165 ± 0.050, 0.109 ± 0.015, 0.175 ± 0.015, and 0.112 ± 0.026 kcal/mol, respectively, at 298, 313, 328, and 348 K). Contact-minimum anti-cooperativity persists at higher temperatures but has reduced magnitudes, with the above measure of anti-cooperativity taking a value of 0.055 ± 0.037 kcal/mol at 368 K. It is noteworthy that the sampling uncertainties for cm at 298, 313, 328, and 348 K are all significantly smaller than the observed anti-cooperative effects. Therefore, aside from $T = 278$ K, at which the sign of cm nonadditivity is not quite certain (-0.046 ± 0.043 kcal/mol), the present simulation dataset exhibits a clear, consistent trend of three-methane anti-cooperativity of 0.1 kcal/mol or more at the contact minimum over a wide temperature range.

The nonadditivity trend at the desolvation barrier (db) appears to be definitive as well (Figure 6). Intriguingly, the barrier height comparison in Figure 6 indicates that the hydrophobic interaction of the methane dimer + single methane system at the $\phi = 0$ desolvation barrier is anti-cooperative at low to intermediate temperatures (three-methane db is 0.12 ± 0.07, 0.24 ± 0.05, and 0.15 ± 0.06 kcal/mol higher than the additivity-assumed db at 278, 298, and 313 K, respectively). But the degree of anti-cooperativity exhibits a clear decreasing trend as temperature is increased from 298 K, and the interaction quite clearly becomes cooperative at 368 K (now the three-methane db is 0.11 ± 0.08 kcal/mol *lower* than the additivity-assumed db).

It should be noted that the nonadditivity measure used in this subsection for cm (above) and db (Figure 6) compares the local minimum of free energy minimum (for cm) or the local maximum of free energy (for db) of the three-methane PMF versus that of the additivity-assumed PMF. The location ξ of each of these key features along the free energy profiles of the three-methane PMF is nearly but not necessarily exactly identical to that of the additivity-assumed PMF (see, e.g., the location of db peaks in Figure 5D−F). Hence, although the nonadditivity measure in this subsection is closely related and has values almost identical to that of the corresponding cooperative term in refs 27 and 49, the two quantities can be slightly different because the cooperative term[27,49] is defined as the difference between three-methane and additivity-assumed PMFs at the same given location, i.e., cooperative term $= \Delta G(\xi,\phi) - \Delta G_{\text{add}}(\xi,\phi)$. The present analysis, on the other hand, focuses more on $\Delta G(\xi,\phi) - \Delta G_{\text{add}}(\xi',\phi)$ as a measure of nonadditivity, where ξ is the cm or db separation for the three-methane PMF and ξ' is the cm or db separation for the additivity-assumed PMF ($\xi' \approx \xi$). This measure is better suited to address certain aspects of physics (e.g., crossing of transition-state-like barriers in protein folding) that require thermodynamic stability information at the local extrema (e.g., height of the barrier) of the actual three-methane versus that of the additivity-assumed free energy landscapes.

C. Three-Methane Thermodynamic Signatures. Given the three-methane PMFs (Figure 3 and data for other ϕ's), thermodynamic signatures of hydrophobic association for every three-methane configuration (position) can be estimated by least-squares fitting the expression in eq 4 to the temperature-dependent PMF values for the given position.[26] Representative examples of this calculation are provided in Figure 7. It is clear from this plot that, in general, the temperature dependences of the PMF for different configurations (cm, db, or ssm in this case) follow quite different trends. These thermodynamic signatures quantify the impact of the nonpolar solutes' spatial arrangement on the physical character of their hydrophobic interactions and facilitate inferences about possible underlying molecular mechanisms.[4,12−14,67−73]

D. Enthalpy and Entropy of Three-Methane Association. The above fitting method (eq 4) is now applied to the entire $\phi = 0$ three-methane PMF profile. The resulting enthalpy (ΔH_0) and entropic free energy ($-T_0\Delta S_0$) of three-methane association at 25 °C are shown in Figure 8 as functions of the distance ξ between the methane dimer and the single methane. The corresponding solvent-accessible surface area (SASA)[15] and

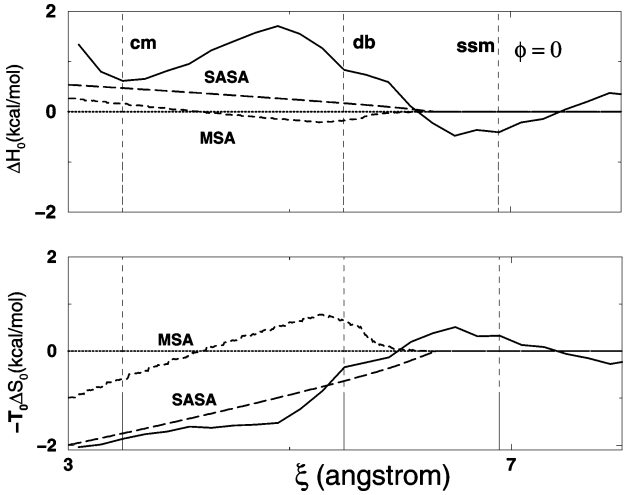

Figure 8. Enthalpy and entropy changes at $T_0 = 298$ K and $\phi = 0$ and the corresponding SASA and MSA predictions based upon simulation data for single-methane hydration (Table 1 and Figure 2). The entropic free energy is shown in the lower panel. Horizontal dotted lines mark the $\Delta H_0 = 0$ and $\Delta S_0 = 0$ levels. The vertical dashed lines mark the approximate ξ positions of contact minimum (cm), desolvation barrier (db), and solvent-separated minimum (ssm). (Note that the exact positions of these features depend weakly on temperature, cf. Figure 3.)

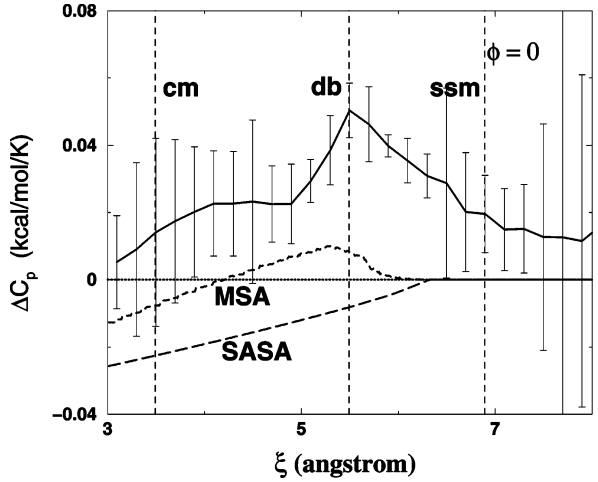

Figure 9. Simulated three-methane heat capacity (solid curve) as a function of the intersolute separation at $\phi = 0$. Error bars for heat capacity are estimated using the formulation in the work of Shimizu and Chan[33] from the sampling uncertainties of the three-methane PMFs that are quantified by the difference between half-simulation and full-simulation results here. The corresponding three-methane heat capacities predicted by SASA (long dashed curve) and MSA (short dashed curve) based on single-methane data are also shown. The horizontal dotted line marks the $\Delta C_P = 0$ level. Vertical dashed lines have the same meaning as in Figure 8.

molecular surface area (MSA)[16] predictions[27] based upon the present single-methane hydration data are included for comparison.

Figure 8 shows that both SASA and MSA fail to account for the large enthalpy increase at $\xi \approx 5$ Å midway between the desolvation barrier and the contact minimum (upper panel). Nonetheless, the SASA prediction comes quite close (and significantly closer than the MSA prediction) to the simulated enthalpy at the three-methane contact minimum. On the other hand, SASA very well captures the ξ dependence of three-methane entropic free energy (lower panel), especially in the region between the desolvation barrier and contact minimum. In contrast, the MSA prediction is far from matching the simulated entropic free energy. Interestingly, the distance-dependent trend exhibited by Figure 8 for three-methane hydrophobic interactions shares substantial similarities with recent calculations of two-methane configuration-dependent enthalpy[75] and entropic free energy[33,75,76] as well as corresponding two-xenon simulations using five common water models.[77]

E. Positive Heat Capacity at the Three-Methane Desolvation Barrier. Figure 9 shows the separation-dependent heat capacity $\Delta C_P(\xi)$ of three-methane hydrophobic association for $\phi = 0$ obtained from the above-described PMF-fitting method.[33] The error bars of the ΔC_P function here are derived from the sampling uncertainties of the PMFs. Because heat capacity is proportional to the second derivative of the free energy (PMF) with respect to T, the uncertainties of ΔC_P estimates are amplified relative to those of the PMFs themselves.

A prominent feature in the three-methane heat capacity function in Figure 9 is the ΔC_P peak value of $\sim$50 cal mol^{-1} K^{-1} near the PMF desolvation barrier. The sampling uncertainties in ΔC_P around this peak are relatively small. Thus, one can be confident that the present model indeed predicts a significant positive ΔC_P there. The heat capacity is also positive, with a lower magnitude of $\sim$10 cal mol^{-1} K^{-1} at the three-methane contact minimum and at the solvent-separated minimum. Neither the SASA nor the MSA implicit-solvent approach provides a quantitatively accurate account of the three-methane $\Delta C_P(\xi)$ function, although the trend of a decreasing ΔC_P from the desolvation barrier to contact minimum is consistent with SASA and MSA predictions. SASA predicts a heat capacity of three-methane hydrophobic interactions that is always negative (long dashed curve in Figure 9). In contrast, the ΔC_P estimated from our PMF simulations is positive for an extended ξ regime. MSA does capture part of the positive heat capcity peak near the PMF desolvation barrier (short dashed curve in Figure 9), but the predicted height of the heat capacity peak is less than 20% of the directly simulated value.

Figure 10 extends the three-methane ΔC_P analysis to other ϕ angles. Despite considerable sampling uncertainties, several general trends are quite clear. For every ϕ angle we have investigated, there is consistently a ΔC_P peak of $\sim$50−65 cal mol^{-1} K^{-1} near the desolvation barrier of the three-methane PMF. And the error bars at these heat capacity peaks are all sufficiently small to support the conclusion that ΔC_P is significantly positive for these configurations. The position of the ΔC_P peak is near the PMF desolvation barrier for small angles ($\phi = 0$, $\pi/12$, and $\pi/6$). But for larger angles ($\phi = \pi/4$, $\pi/3$, and $5\pi/12$), the ΔC_P peak shifts toward the contact minimum (position marked by the leftmost vertical dashed lines in each panel of Figure 10). In the present simulation, the contact minimum has a positive ΔC_P that appears to increase with ϕ, from <20 cal mol^{-1} K^{-1} at $\phi = 0$ to >50 cal mol^{-1} K^{-1} at $\phi = 5\pi/12$. As far as common implicit-solvent treatments of ΔC_P are concerned, Figure 10 indicates that both SASA and MSA are unable to account for the intricate configuration-dependent heat capacity of three-methane hydrophobic association.

IV. Discussion

A. Beyond Bulk-Phase Considerations of Hydrophobicity. The SASA and MSA predictions in Figures 8 and 9 above are based upon simulated single-methane data. They correspond to the common approach of using bulk-phase model compound solvation to understand hydrophobic effects.[6] Therefore, the

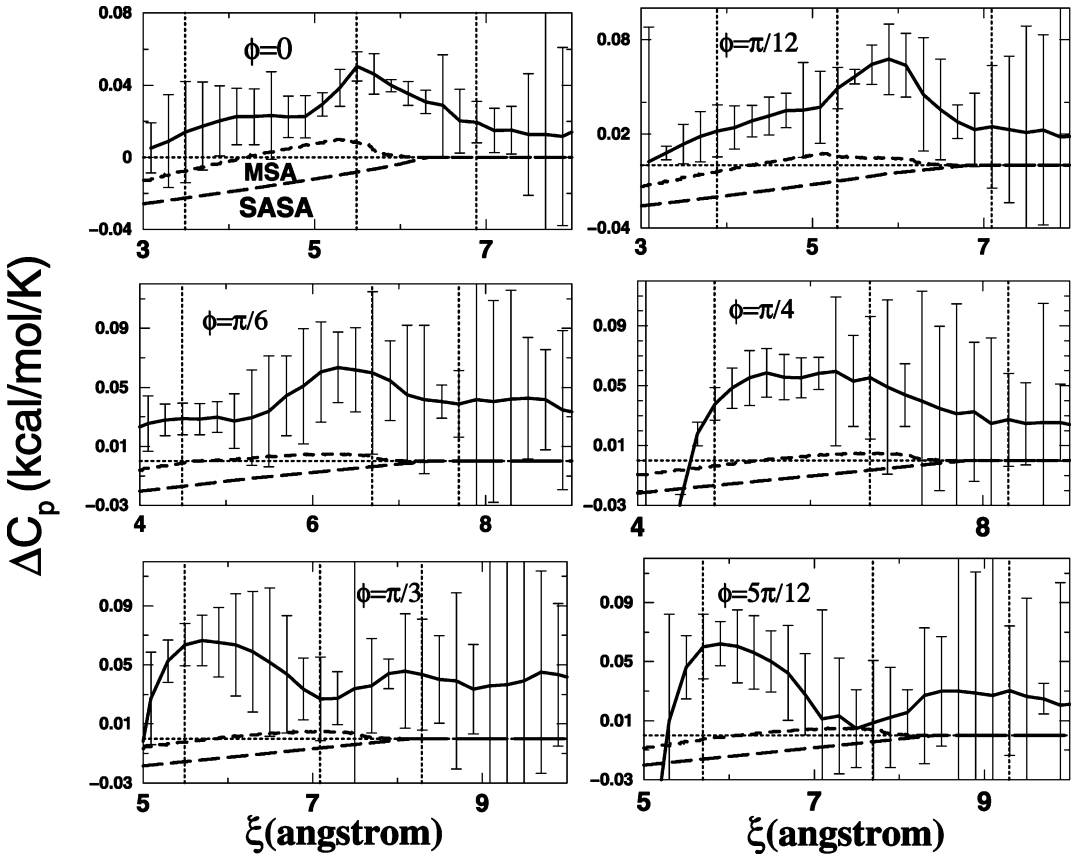

Figure 10. Three-methane heat capacity for different ϕ angles. The directly simulated three-methane heat capacities (solid curves) are compared with SASA (long dashed curves) and MSA (short dashed curves) predictions based upon the simulated hydration heat capacity of a single methane. The vertical lines mark the approximate ξ positions (from left to right) of contact minimum, desolvation barrier, and solvent-separated minimum for the given ϕ. The horizontal dotted lines mark the $\Delta C_P = 0$ level. Error bars are derived from the sampling uncertainties of the ϕ- and T-dependent three-methane PMFs using the same method as in Figure 9 above. The $\phi = 0$ data from Figure 9 are included here for comparison, whereas the $\phi = \pi/2$ heat capacity estimates contain large uncertainties and thus are not shown.

comparison between directly simulated three-methane data and SASA/MSA predictions in these plots can be used to assess the validity of such bulk-phase approaches. In this regard, Figure 8 shows that SASA has some limited successes. As noted above, at the three-methane contact minimum, the enthalpy change (>0) and entropy change (<0) upon hydrophobic association (from directly simulated PMF data) at room temperature (298 K) have the same sign and approximately the same magnitude as the corresponding SASA predictions. On the other hand, however, Figure 9 demonstrates clearly that the three-methane enthalpy and entropy's temperature dependence (governed by ΔC_P) has signs opposite to that predicted by SASA. Similar features have also been observed for two-methane hydrophobic association.[26,33,34] Taken together, these results imply that the common SASA picture derived from bulk-phase hydrophobicity is generally not adequate for understanding the hydrophobic interactions among a small number of nonpolar solutes.

This mismatch between bulk-phase and few-solute hydrophobic interactions is further highlighted by the temperature-dependent enthalpy, $\Delta H(T) = \Delta H_0 + (T - T_0)\Delta C_P$, and entropy, $\Delta S(T) = \Delta S_0 + \Delta C_P \ln(T/T_0)$, of three-methane hydrophobic association in Figure 11. The "1met" curves in this figure provide for comparison of the enthalpy and entropy changes that accompany the removal of a single methane from water, which corresponds to bulk-phase desolvation. The "1met" process entails a positive enthalpy change (unfavorable), a positive entropy change (favorable), and a significant negative heat capacity change at room temperature (298 K). At higher temperature, the "1met" enthalpy change switches sign to become negative, and the entropy change becomes less positive. This thermodynamic trend corresponds to a traditional hallmark of hydrophobicity.[68] However, the temperature variation of the enthalpy and entropy at the three-methane desolvation barrier exhibits an opposite trend (Figure 11). A similar behavior applies also to the two-methane desolvation barrier[26] (data not plotted). Here, Figure 11 shows that the enthalpy and entropy at the three-methane contact minimum and solvent-separated minimum also do not follow the "1met" temperature dependence trend. These findings imply that bulk-phase desolvation cannot be used to model the physics of partial "desolvation" or clustering of a small group of nonpolar solutes that are otherwise also partially solvent exposed.

B. Ramifications for Protein Folding. The more intricate features of hydrophobic interactions revealed by the present three-methane study provide new insights into protein energetics and conformational distribution. In our view, recognizing the significant differences between bulk-phase hydrophobicity and the hydrophobic interactions among a small cluster of small-sized nonpolar solutes is critical for a better physical understanding of protein behavior. Some of these differences have been noted in our previous two-methane simulations.[33,34,36] The present results make a step forward in indicating that many of the non-bulk-like features of two-methane hydrophobic interactions persist in the three-methane situation as well. Hence, it is

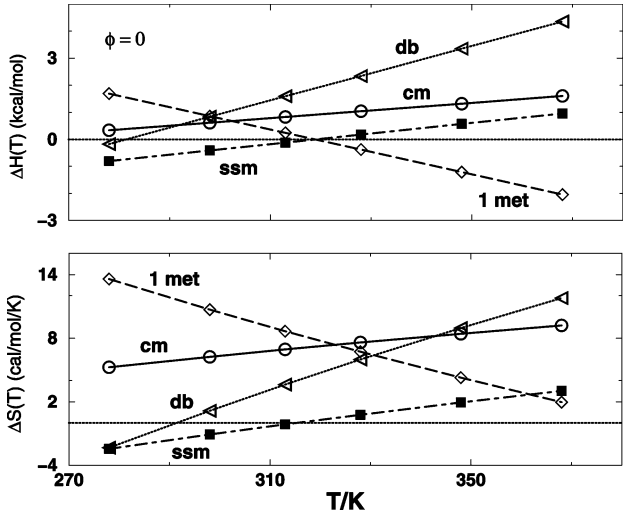

Figure 11. Enthalpy and entropy changes as a function of temperature at the contact minimum (cm, circles), desolvation barrier (db, triangles), and solvent-separated minimum (ssm, squares) (as defined in Figure 8) of the $\phi = 0$ three-methane PMF. Temperature dependence (continuous curves) is computed using the fitted thermodynamic parameters obtained in this work (Figure 7, top panel). The enthalpy and entropy changes upon the desolvation (removing from water) of a single methane are also plotted for comparison ("1met", diamonds). Note that the thermodynamic signatures of the present "1met" process are minus that of the reverse process of inserting a single methane into water. The symbols along the curves here serve merely as guides for the eye.

appropriate to generalize the distinctions between "pair" and "bulk" hydrophobic effects[23] to that between "small-cluster" and bulk-phase hydrophobic interactions.

Obviously, any relationship between explicit-water simulations of a small number of nonpolar solutes and the complex phenomenon of protein folding is necessarily indirect. As in bulk-phase model compound approaches, the connections between small-molecule and protein-folding processes are merely intuitive in nature and at best semiquantitative.

Nonetheless, as far as conceptual advances are concerned, the theoretical possibilities offered by our new small-cluster simulations are valuable, as many scenarios suggested by our newly gained insights were unavailable within the traditional bulk-phase paradigm. Several such scenarios for rationalizing experimental protein folding data are outlined below.

One generic feature of the temperature dependence of protein folding kinetics is that it is often non-Arrhenius, with a peak folding rate at an intermediate temperature.[90−92] In other words, as a function of temperature, the free energy barrier height has a minimum, and the function becomes concave upward. Hence, in such cases, the protein's folding transition state has a negative heat capacity. In view of the importance of solvation effects in protein folding energetics, it is reasonable to expect mechanisms closely related to those that give rise to desolvation barriers in small-molecule PMFs to play an important role in the overall free energy barrier to protein folding. Motivated by this rationale, researchers have recently used pairwise desolvation free energy barriers to provide insights into aspects of protein thermodynamics, cooperativity, and folding kinetics.[28−30,45,93] The present three-methane study is pertinent to this line of investigation. Fundamentally, our results show that desolvation free energy barriers are generally nonadditive, and that the temperature dependence of the sign and magnitude of nonadditivity can lead to further energetic complexities as well. In light of these findings, it would be instructive to explore how this and similar nonadditivity phenomena may be utilized to gain a deeper understanding of the temperature dependence of protein folding and unfolding kinetics.[29,94]

As for the heat capacity signatures of free energy barriers, both our previous two-methane[26,33,34] and the present three-methane (Figures 9 and 10) desolvation barrier heat capacities are positive, i.e., have signs opposite to that of a typical transition-state heat capacity of protein folding. Recently, several other research groups have also investigated the separation-dependent two-body heat capacity of association of a pair of nonpolar solutes.[40,76−78] While the overall magnitude of the heat capacity profile[76] and the sign of heat capacity at the contact minimum appear to be sensitive to the size of the nonpolar solute[40,77] and the water model,[77] a positive heat capacity peak near the PMF desolvation barrier emerges as a robust feature observed across several studies of heat capacity of pairwise small nonpolar solute association.[26,33,34,40,76−78,95]

Quite remarkably, the newly obtained heat capacity of three-methane association in Figure 9 exhibits a profile very similar to that of the two-methane heat capacity, suggesting that their physical origins[78] may be closely related. Taken together, the two- and three-body heat capacity simulation data acquired to date strongly indicate that the typical rate-limiting step in protein folding is quite different from surmounting two-methane-like or three-methane-like desolvation barriers, or a simple addition of many such processes. The folding transition state generally involves simultaneous interactions among a larger number of bigger chemical groups. In this context, it would be interesting to investigate whether the PMF desolvation barriers of bigger solutes, such as neopentane[34] and entire amino acid side chains,[30] would afford heat capacity signatures that are more akin to the typical protein folding transition state.

This perspective from two- and three-body simulation results may also be relevant to the understanding of compact denatured states of proteins.[96] Protein conformations have been found to be relatively compact in heat-denatured states,[97,98] and in certain unfolded states under non-denaturing conditions.[99] The nonpolar SASA of some molten-globule-like compact denatured states is significantly smaller than that of the fully unfolded state. Therefore, in the traditional view, the heat capacity (ΔC_P) of such compact denatured states of a protein is expected to be markedly less than that of the fully unfolded state. However, at least for two proteins, when conditions become more favorable to the native state, the progress of the ΔC_P signature (from a

(90) Segawa, S.-I.; Sugihara, M. *Biopolymers* **1984**, *23*, 2473−2488.
(91) Jackson, S. E.; Fersht, A. R. *Biochemistry* **1991**, *30*, 10428−10435.
(92) Schindler, T.; Schmid, F. X. *Biochemistry* **1996**, *35*, 16833−16842.
(93) Fernandez-Escamilla, A. M.; Cheung, M. S.; Vega, M. C.; Wilmanns, M.; Onuchic, J. N.; Serrano, L. *Proc. Natl. Acad. Sci. U.S.A.* **2004**, *101*, 2834−2839.
(94) Day, R.; Bennion, B. J.; Ham, S.; Daggett, V. *J. Mol. Biol.* **2002**, *322*, 189−203.
(95) The heat capacity values estimated from the two-methane data in Figure 5 for the contact minimum (cm) and desolvation barrier (db) exhibit trends similar to the corresponding two-xenon/TIP4P heat capacity values determined recently by Paschek.[77] While the two-methane ΔC_P values we obtained here with increased sampling are lower (more negative at cm and less positive at db) than our previous estimates,[26,33,34] the feature of a positive two-methane desolvation heat capacity is confirmed.
(96) Shortle, D. *FASEB J.* **1996**, *10*, 27−34.
(97) Sosnick, T. R.; Trewhella, J. *Biochemistry* **1992**, *31*, 8329−8335.
(98) Seshadri, S.; Oberg, K. A.; Fink, A. L. *Biochemistry* **1994**, *33*, 1351−1355.
(99) Mok, Y. K.; Kay, C. M.; Kay, L. E.; Forman-Kay, J. *J. Mol. Biol.* **1999**, *289*, 619−638.

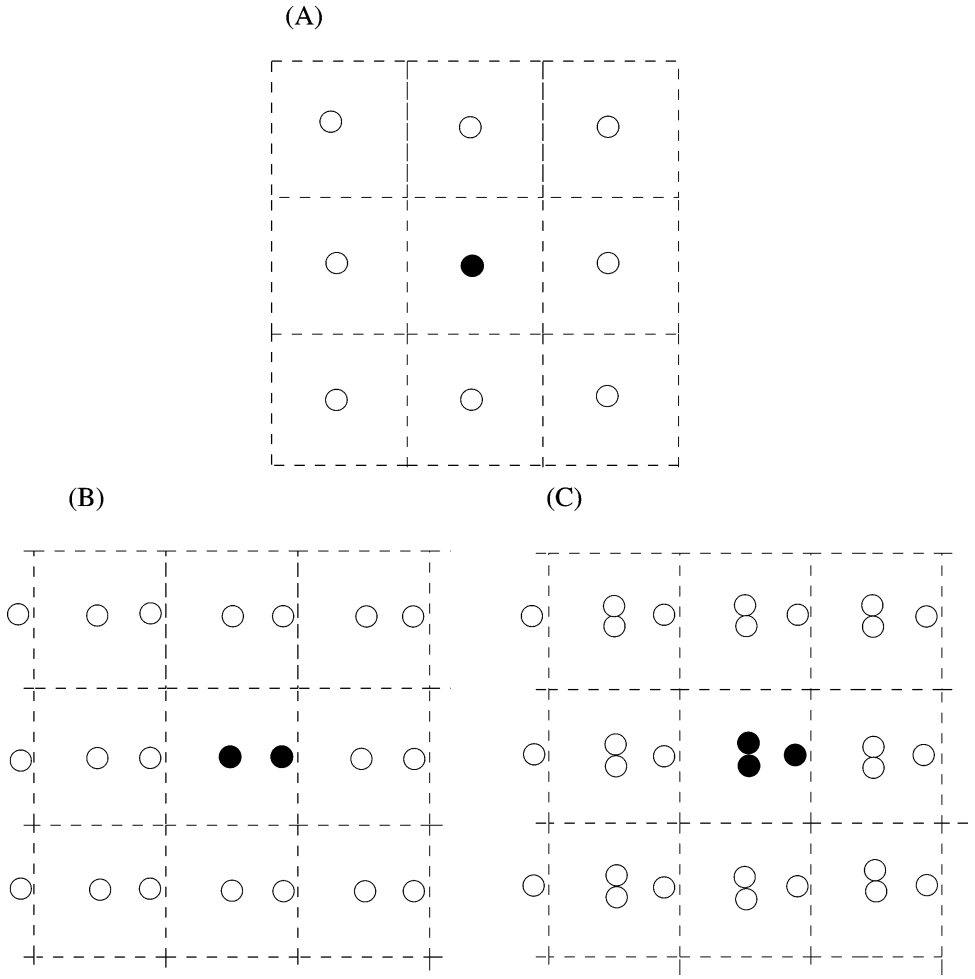

Figure 12. Effects of periodic boundary conditions on the determination of zero-PMF baseline. Solutes are denoted by filled circles in a simulation box of water molecules (not depicted explicitly); image solutes are shown as open circles. (A) Zero-PMF baselines for two- and three-methane PMFs are determined by test-particle insertions of a single methane in pure water. This is the method used in the present work. In contrast, the zero-PMF baselines in some studies of (B) two- and (C) three-methane PMFs are set by postulating that hydrophobic interaction is nonexistent at a finite distance considered to be "far apart" in the simulation box (e.g., configurations in panels B and C). In these drawings, the ratio of solute size to the dimension of the simulation box corresponds roughly to that in the present methane simulations and similar simulations reported in the literature (see text for details).

higher unfolded value to a lower folded value) appears to lag behind that of other measures such as helicity and radius of gyration. The ΔC_P value decreases sharply only at the last stage of folding, i.e., in the transition from a molten-globule-like state to the native state, suggesting that tight packing is necessary for achieving the native ΔC_P signature.[100,101] This observation would be rather puzzling in the bulk-phase SASA view. In contrast, it may be rationalizable by the following hypothesis based on the present three-methane heat capacity results and similar trends for two-methane heat capacity:[34] The positive heat capacity values in Figures 9 and 10 for three-methane hydrophobic association imply that hydrophobic contacts per se do not necessarily lower heat capacity when the contacting nonpolar solutes are still partially yet significantly exposed to water. Thus, consistent with experimental observations,[100,101] a lowering of ΔC_P would occur only when there are either a larger number of nonpolar solutes or larger-sized nonpolar solutes coming together, or both. In other words, a crossover from small-cluster to bulk-like hydrophobic behavior would not ensue until multiple nonpolar groups are sequestered from water in a hydrophobic core.

C. Computational Accuracy and the Estimation of Zero-PMF Baselines in Nonadditivity Analyses. We now turn to several critical computational issues related to the numerical reliability of the present study and assess them in some detail. To date, two main approaches have been used in the investigation of hydrophobic nonadditivity to estimate zero-PMF baselines:[26] (i) Setting the zero-PMF value by test-particle insertion into pure solvent;[26,27,33,66,77] this is the method used in the present study. (ii) Identifying the zero-PMF baseline with a certain average PMF value at large intersolute separations within the given simulation box if the large-separation PMF values are found to be "flat" or nearly so, i.e., essentially independent of position.[48,53,56] For brevity, we refer to this procedure as the "large-separation" method. The basic physical premise for both methods is the same, namely that PMF should decay to zero at infinite separation. In principle, this means that the zero-PMF baseline can be determined by using a very large simulation box. However, because computational resources are necessarily limited, simulation boxes are often not very large relative to the size of the solutes under consideration (cf. Figure 12). The

(100) Nishii, I.; Kataoka, M.; Tokunaga, F.; Goto, Y. *Biochemistry* **1994**, *33*, 4903−4909.
(101) Nishii, I.; Kataoka, M.; Goto, Y. *J. Mol. Biol.* **1995**, *250*, 223−238.

two methods thus represent different attempts to utilize limited simulation data to arrive at a reasonable estimate of the true zero-PMF baseline.

Figure 12 considers the potential artifacts of these two methods. Under periodic boundary conditions, a solute and an image solute can exert influence on each other via intervening solvent (water) molecules even when the solute−image−solute separation is larger than the cutoff distance for direct interactions. Hence, strictly speaking, the test-particle insertion method does not provide the exact hydration free energy at infinite solute dilution, but rather the hydration free energy at a finite nonzero solute concentration dictated by the size of the simulation box (Figure 12A). Nonetheless, for simulations using a given box size (say, of linear dimension L), the test-particle insertion method offers a more accurate estimate of the zero-PMF baseline because the image solutes in the single-solute calculation are always at least at a distance L away from the solute itself (Figure 12A). In contrast, for the "large-separation" method, when the solutes themselves are maximally separated or nearly so in the simulation box (i.e., $\xi \approx L/2$), a solute is only $\sim L/2$ away from the closest image solute (Figure 12B,C). This distance is half of the separation between a solute and a closest image solute in Figure 12A; hence, the influence of the image solute on the energetics is bound to be less negligible in the "large-separation" method. It follows that Figure 12B,C is a worse model for infinite intersolute separation than Figure 12A. For the three-methane case, the image solutes would be even more influential because when the single methane solute is $\sim L/2$ away from the methane dimer, it is only $\sim L/2$ away from the image of a methane dimer at the same time (Figure 12C). Therefore, although the test-particle insertion method is imperfect, it is a better approximation of ideal infinite intersolute separation than the application of the "large-separation" method to a simulation box of the same size. Indeed, the above analysis suggests that for a "large-separation" PMF baseline to be as accurate as that obtained using the test-particle insertion method, the linear dimension of the simulation box employed by the "large-separation" method needs to be at least double that for the test-particle insertion method. In other words, approximately 8 times as many molecules are required for the "large-separation" as for the test-particle method.

The linear dimension of the simulation box used in the present study is ∼23 Å (396 waters). This is somewhat smaller than the linear dimensions of simulation boxes used in other investigations of three-methane hydrophobic interactions to date, viz., Rank and Baker, ∼25 Å (515 waters);[45] Ghosh et al., ∼25 Å (508 waters) and ∼32 Å (1016 waters);[55] and Czaplewski et al., 28 Å (∼692 waters).[56] Therefore, for reasons outlined above, we believe that our zero-PMF baseline obtained using the test-particle insertion method is more reliable than those obtained in these other studies using the "large-separation" method, since none of them used a simulation box size of ∼46 Å or larger. In the case of Ghosh et al.,[55] the accuracy of their zero-PMF baseline is expected to be further compromised because their simulation boxes contain 10 or 20 methanes instead of just one, two, or three methanes.

Two further implications of edge effects of finite simulation boxes are noteworthy. First, the existence of artifactual indirect (solvent-mediated) interactions between solutes and image solutes means that PMF results for larger separation are less reliable than PMF results for smaller separation, even when the test-particle insertion method is used to determine the zero-PMF baseline.[27] Because of this, in some cases only results for relatively smaller intersolute separations are shown in the present study. Second, and more importantly, edge-effect considerations point to an additional pitfall of the "large-separation" method, which stipulates that an observed flatness of PMF at large separations is sufficient to justify the assumption that the PMF has reached its asymptotic zero value.[56] Physically, a flat PMF only implies that the mean force is zero. It says nothing about the absolute value of the PMF relative to the true zero-PMF value at infinite separation. In fact, when the intersolute separation approaches its maximum value in the simulation box as in Figure 12B,C, the resulting geometric symmetry of the system means that the solvent-mediated influence on a given solute by the other solutes in the simulation box itself would be essentially canceled by the influence from the image solutes. So, the net mean force experienced by the solute at an edge of a simulation box can be zero, even though the mean force acting on it by the other solutes in the simulation box (image solutes excluded) is in fact nonzero. Therefore, an apparent flatness of the simulated PMF at large separations may only be a consequence of the periodic boundary condition and cannot by itself be used to prove that the PMF itself is zero at those separations.

D. Anti-Cooperativity of Three-Methane PMFs at 298 K and 1 atm: Comparison of Results from Different Studies. Simulations of three-methane hydrophobic interactions and nonadditivity effects to date have not addressed temperature dependence, aside from a very brief discussion of a possible crossover from mainly anti-cooperative to cooperative behavior when temperature is increased from 25 to 95 °C (ref 27). Inasmuch as we are aware, three-methane PMFs at ∼25 °C were previously simulated by four research groups. Table 2 summarizes some of the most recent results. Our prediction of three-methane anti-cooperativity at 25 °C and 1 atm[27] is in partial agreement with the earlier findings of Rank and Baker[45] as well as a subsequent study by Ghosh et al.;[55] both of these research groups performed constant-pressure simulations and found anti-cooperativity at the three-methane contact free energy minimum. But we are in apparent disagreement with Czaplewski et al., who have concluded from their constant-volume simulations that three-methane interaction is cooperative[48] or almost additive.[56]

Table 2 provides a comparison of free energy differences between key positions along the two- and three-methane PMF profiles. These quantities are relative free energies. Thus, they are independent of the choice of zero-PMF baseline: If pairwise additivity is applicable, the free energy difference between two different configurations of a pair of methanes must equal to one-half of the corresponding free energy difference for the three-methane (methane dimer + methane) system. The data in Table 2 indicate that pairwise additivity does not apply for three-methane hydrophobic interactions at ∼25 °C. In fact, one anti-cooperative aspect of these simulation results appears to be robust across the different studies: In all four cases, the free energy difference between the two-methane contact minimum and desolvation barrier (first row of entries) is larger than one-half of the corresponding free energy difference for three methanes (third row of entries). It follows that three-methane

Table 2. Comparison of Studies of Three-Methane Nonadditivity at Temperature $T \approx 25$ °C in the $\phi = 0$ Configuration[a]

study	Rank and Baker (1997)	Shimizu and Chan (2002)	Ghosh et al. (2003)	Czaplewski et al. (2003)
water model	TIP4P	TIP4P	TIP3P	TIP3P
simulation ensemble	*NPT*	*NPT*	*NPT*	*NVT*
	$T = 298.15$ K	$T = 298.15$ K	$T = 300$ K	$T = 298$ K
two-methane: $PMF^{(2)}$ (db)−$PMF^{(2)}$ (cm)	0.92[b]	0.84[d]	0.98[e]	0.99[g]
two-methane: $PMF^{(2)}$ (db)−$PMF^{(2)}$ (ssm)	0.29[b]	0.31[d]	0.31[e]	0.32[g]
three-methane ($\phi = 0$): $PMF^{(3)}$ (db)−$PMF^{(3)}$ (cm)	1.64[c]	1.76[d]	1.55[f]	1.92[h]
three-methane ($\phi = 0$): $PMF^{(3)}$ (db)−$PMF^{(3)}$ (ssm)	0.79[c]	0.61[d]	0.51[f]	0.64[h]

[a] Approximate free energy differences (in kcal/mol) in two- and three-methane PMFs between the desolvation barrier (db) and the contact minimum (cm), and between db and the solvent-separated minimum (ssm), are estimated from published figures in four studies. *NPT* simulations results here are for pressure $P = 1$ atm. [b] Figure 2A of ref 45. [c] Figure 4A of ref 45. [d] Figure 12 of ref 27. [e] 1.0 atm curve in Figure 1 of ref 55. [f] $W^{(3)}$ curve in Figure 6a of ref 55. [g] PMF from the longest run in Figure 2 of ref 56. [h] PMF from the longest run in Figure 3 of ref 56.

hydrophobic interaction for $\phi = 0$ has to be either anti-cooperative at the desolvation barrier or anti-cooperative at the contact minimum, or both, depending on the choice of zero-PMF baseline. But irrespective of the choice of baseline, this observation implies that the interaction cannot be cooperative at both the contact minimum and the desolvation barrier.

Interestingly, an informational theory investigation by Hummer et al.[102] also supports three-methane anti-cooperativity under the same set of conditions. Instead of directly simulating the water-mediated interactions among methanes, their method was based on the formation probabilities of methane-sized cavities in simulated ensembles of pure water (256 SPC model waters) under a range of different pressures (−16 to 725 MPa) at 298 K. Although the authors remarked that their three-body PMFs (in equilateral configurations) were well approximated by the sum of their two-body PMFs,[102] a simple comparison of Figures 2 and 3 in this reference indicates that, at low pressure (∼1 atm), the desolvation barrier is in fact slightly anti-cooperative by ∼0.1 kcal/mol, whereas the contact minimum is essentially additive.

At this juncture, it is instructive to compare and assess two recent three-methane simulations in more detail in light of the analysis of edge effects in the last subsection. Ghosh et al.[55] reported anti-cooperativity for the contact and solvent-separated minima at 300 K under *NPT* conditions (1 atm, methanes in water without salt) using the TIP3P model for the $\phi = 0$ case. This conclusion is consistent with our previous finding based on the TIP4P model.[27] However, contrary to our observation of significant anti-cooperativity at the desolvation barrier at 298 K (Figures 5 and 6), Ghosh et al. reported a cooperative effect at the desolvation barrier. One possible cause of this disagreement is the difference in water models, and this is an issue that remains to be better understood.[103] As far as PMF baselines are concerned, the zero-PMF value in Ghosh et al.'s approach was set by their choices for the normalization of the methane correlation functions. Effectively, PMF values were simply assumed to be essentially zero at the edge of their simulation box. As such, their method does not address the possibility of long-range hydrophobic effects.[81]

Czaplewski et al.,[56] on the other hand, found that under *NVT* conditions three-methane hydrophobic interactions in their "$2m + m$" configurations (equivalent to our $\phi = 0$) are slightly anti-cooperative both at the contact minimum and at the desolvation barrier at 298 K in the TIP3P model (Figure 4 of ref 56). Their calculation was based on an assumption that both the two-methane and three-methane PMFs are essentially zero at separation $\xi \approx 12$ Å. Summarizing their findings, the authors asserted that "a pairwise approximation of the PMF seems to be almost sufficient" for the interactions of three methanes in water.[56] This assessment is different from the research group's previous conclusion that the same three-methane interaction was mainly cooperative (12-window result in Figure 8A of ref 48). A possible cause for this difference is that the two studies employed different PMF baselines: Instead of assuming that PMF = 0 at $\xi \approx 12$ Å (ref 56), the earlier study assumed that the actual three-methane PMF and the hypothetical PMF based upon pairwise additivity of two-methane PMFs should coincide in the region of 7.5−8.5 Å separation.[48] But this procedure is problematic.[52] Now, results in the more recent report by Czaplewski et al.[56] indicate that their 12 Å criterion also may not be sufficiently accurate. This can be seen readily by noting the inconsistency in their "$2m + m$" and "$m + m + m$" plots. For the longest simulation runs reported, the free energy at the contact minimum for the "$2m + m$" case is ~ -0.74 kcal/mol (relative to the assumed zero-PMF baseline at ∼12 Å; see Figure 3a and the first panel of Figure 4 of ref 56). In contrast, the corresponding free energy for the "$m + m + m$" case is ~ -0.83 kcal/mol (Figure 3b and second panel of Figure 4 of ref 56). Since the three-methane contact minimum configuration is the same for "$2m + m$" and "$m + m + m$" (with all intermethane distances equal to the contact minimum between two methane molecules in water[48]), it follows from the basic principles of thermodynamics that their free energies relative to the infinite-separation situation should be identical. Therefore, the fact that the assumed 12 Å PMF baseline gave rise to an ∼0.09 kcal/mol discrepancy in free energy for these two cases implies that the assumed baseline does not correspond to the absolute zero PMF value. So, in these simulations, it appears that even a separation of 12 Å is insufficient for the methanes to be truly independent of one another (cf. Figure 12).

(102) Hummer, G.; Garde, S.; Garcia, A. E.; Paulaitis, M. E.; Pratt, L. R. *Proc. Natl. Acad. Sci. U.S.A.* **1998**, *95*, 1552−1555.

(103) We note that Ghosh et al.'s reported anti-cooperativity at the contact minimum and cooperativity at the desolvation barrier do not appear to add up to the values summarized in Table 2 above.

V. Concluding Remarks

To summarize, we have completed a first study of the temperature dependence of hydrophobic interactions between a single methane and a methane dimer, using extensive Monte Carlo sampling and test-particle insertion techniques to obtain more reliable zero-PMF baselines. The three-methane PMFs exhibit a significant dependence on temperature. The present investigation employs only the TIP4P water model. As such, the robustness of our conclusions across different common water models[77] remains to be ascertained. Nonetheless, the findings here provide rudimentary insights into complex water-mediated interactions among a small cluster of nonpolar solutes. In general, three-methane hydrophobic interactions are not pairwise additive. Generalizing our previous conclusions[27] for 25 °C, here we have determined the temperature dependence of this pairwise nonadditivity. In particular, the three-methane desolvation barrier is shown to be anti-cooperative at low to intermediate temperatures, but shifts to essentially additive or slightly cooperative at high temperatures, whereas the contact minimum is anti-cooperative over a broader temperature range. Intuitions based upon bulk-phase hydrophobic effects and solvent-accessible surface area (SASA) are insufficient for grasping the subtleties of small-cluster hydrophobic interactions. The heat capacity function $\Delta C_P(\xi,\phi)$ of three-methane hydrophobic association is strongly configuration dependent. As for the two-methane case,[33,34,36,77] three-methane ΔC_P has a significantly nonmonotonic dependence on the intersolute (inter-methane) separation, with a prominent positive ΔC_P peak near the PMF desolvation barrier (for small ϕ) or the contact minimum (for large ϕ). Thus, burial of nonpolar surface or formation of nonpolar contacts does not necessarily lead to a decrease in heat capacity. This phenomenon—which is not predicted by bulk-phase/SASA considerations—provides a plausible novel rationalization for the heat capacity signature of certain protein compact denatured states. It would be interesting to further explore the molecular basis[78] of this peculiar property of small-cluster hydrophobic interactions.

Acknowledgment. The research reported herein was supported by the Canadian Institutes of Health Research (CIHR grant no. MOP-15323), PENCE, and a Premier's Research Excellence Award from the Province of Ontario. H.S.C. holds a Canada Research Chair in Biochemistry.

JA040165Y